Catalysis Today xxx (2016) xxx–xxx

Contents lists available at ScienceDirect

Catalysis Today

journal homepage: www.elsevier.com/locate/cattod

Effect of reducing agent on the structure and activity of manganese oxide octahedral molecular sieve (OMS-2) in catalytic combustion of *o*-xylene

Yinsu Wu [a], Rui Feng [a], Chaojie Song [b], Shengtao Xing [a], Yuanzhe Gao [a], Zichuan Ma [a,*]

[a] College of Chemistry and Material Science, Hebei Normal University, Shijiazhuang 050024, China
[b] Energy, Mining and Environment, National Research Council Canada, 4250 Wesbrook Mall, Vancouver, BC, V6T 1W5, Canada

ARTICLE INFO

Article history:
Received 25 December 2015
Received in revised form 22 March 2016
Accepted 5 May 2016
Available online xxx

Keywords:
OMS-2
Oxygen vacancy
o-Xylene
Catalytic combustion

ABSTRACT

Manganese oxide octahedral molecular sieve (OMS-2) with different microstructures were synthesized via simple wet chemical methods of $KMnO_4$/benzyl alcohol and $KMnO_4$/$Mn(NO_3)_2$ at room-temperature (the products were denoted as B-OMS-2 and N-OMS-2, respectively). The physicochemical properties of the materials were characterized using numerous analytical techniques. The catalytic activities of the catalysts were evaluated for the complete catalytic oxidation of a typical volatile organic compound (VOCs), *o*-xylene. It was found that B-OMS-2 presented a loose structure, and contained almost 100% Mn^{4+}, while N-OMS-2 possessed a mixture of Mn^{4+} and Mn^{3+}. H_2-TPR and O_2-TPO analyses showed that B-OMS-2 exhibited good low-temperature reducibility and high oxygen exchange ability with gas phase oxygen. The microstructure difference was caused by different reducing reagents used in the synthesis. Benzyl alcohol might adsorb on the surface of MnO_2 nuclei acting as a ligand and/or structure-directing agent, and the desorption of the organic compound led to the formation of bulk oxygen vacancy in B-OMS-2. B-OMS-2 could convert 100% *o*-xylene into CO_2 at 190 °C at a space velocity of 8000 h^{-1}, 50 °C lower than N-OMS-2. The excellent catalytic performance of B-OMS-2 might be caused by its bulk oxygen vacancy, potent reducibility and high re-oxidation ability. It is believed that B-OMS-2 is a promising catalyst for the elimination of VOCs from air.

1. Introduction

Volatile organic compounds (VOCs) such as benzene, toluene, and xylene (BTX) are harmful to the environment. It is highly desirable to remove these pollutants [1–3]. Complete catalytic oxidation techniques converting organic compound contaminants into CO_2 and H_2O are an effective pathway to control VOC emissions [4].

Manganese oxide, such as MnO_2 has been considered as an efficient catalyst for complete catalytic oxidation of VOCs [5–8]. The cryptomelane-type octahedral molecular sieve (OMS-2), MnO_2 with a one-dimensional tunnel structure composed of 2×2 edge shared MnO_6 octahedral chains, has received appreciable attention due to its excellent catalytic performance [9]. However, at low temperature, OMS-2 has lower catalytic activity toward benzene type materials' oxidation than precious metals [10]. To improve OMS-2's catalytic activity, several strategies have been proposed including decreasing the particle size or increasing the surface area [11], doping K^+ in OMS-2 channels [5], substituting part of the Mn with V, Cu, and Fe ions [12], controlling the morphology of OMS-2 [10], and increasing the oxygen vacancy defect concentration in OMS-2 [7,13].

It is commonly accepted that OMS-2 catalyzes VOCs oxidation via the Mars-van Krevelen mechanism. Organic molecules adsorbed on the catalyst surface are oxidized by surface lattice oxygen, and the resultant oxygen vacancies are subsequently replenished by gas-phase O_2 [4]. According to this mechanism, the reducibility or activity of lattice oxygen and re-oxidation ability of OMS-2 appear to be two critical parameters determining their catalytic performance for VOC oxidation.

In the OMS-2 synthesis, reactants usually influence OMS-2 microstructure, and oxygen vacancy concentration and types, which affect the mobility of lattice oxygen, the re-oxidation ability of OMS-2 and interface between VOCs, gas oxygen and OMS-2 [13,14]. The microstructure of MnO_2 is mainly determined by the rate of nuclei growth (governing the formation of building blocks for desired structures) and the extent to which the building blocks

* Corresponding author.
E-mail addresses: mazc@vip.163.com, mazc@hebtu.edu.cn (Z. Ma).

http://dx.doi.org/10.1016/j.cattod.2016.05.024
0920-5861/

aggregate or assemble. The aggregation process plays an important role in tailoring the features of the morphology and porous structure in the product. Usually, the growth of primary structures is modulated by preferential adsorption of anions, solvent molecules, and reaction conditions such as temperature etc. [15]. Usually, OMS-2 materials are prepared by reducing $KMnO_4$ with various inorganic compounds such as Mn(II) salts [16–18]. Recently, OMS-2 with porous and/or three-dimensional frameworks was prepared by reducing $KMnO_4$ with some oxygen-containing organic compounds, such as benzyl alcohol and ascorbic acid [19,20]. In a $KMnO_4$/organic reducing agent system, the organic reducing agent probably not only result in a two-phase synthesis process to control the reaction rate, but also can act as structure-directing to control the growth of nuclei and further influence its microstructure. So far a comparison between the two methods has not been studied yet.

In this paper, we studied the effect of reducing agent (organic compound, and inorganic compound,) on OMS-2 structure and catalytic activity toward VOCs complete oxidation. The OMS-2 synthesized via benzyl alcohol at room temperature was denoted as B-OMS-2, and that prepared by $Mn(NO_3)_2$ at the same condition was denoted as N-OMS-2. Their properties were characterized and catalytic activities toward the complete catalytic oxidation of *o*-xylene were tested. The correlation between catalytic performance and microstructure was analyzed.

2. Experimental

2.1. Synthesis of B-OMS-2 and N-OMS-2

20 mmol benzyl alcohol was added dropwise to a 20 mmol $KMnO_4$ solution. After the mixture was vigorously stirred at room temperature for 24 h, a black product was obtained. The product was washed several times with deionized water and absolute alcohol to remove any possible residual reactants, dried at 110 °C for about 12 h, and then calcined in air at 400 °C for 6 h. The product was denoted as B-OMS-2.

For comparison, OMS-2 was also prepared by reducing $KMnO_4$ with $Mn(NO_3)_2$ at the same conditions as that used in $KMnO_4$-benzyl alcohol. The product was denoted N-OMS-2.

2.2. Catalytic activity evaluation

Catalytic activity was measured in a 4 mm i.d. quartz tubular reactor. 0.50 g of catalyst supported by quartz wool was placed in the center of the reactor. Simulated air (20 vol.% O_2, 80 vol.% N_2) containing 500 ppm of *o*-xylene in continuously passed through the catalyst bed at a flow rate of 50 mL/min (W/F = 0.60 g s mL^{-1}), corresponding to a GHSV of 8000 h^{-1}. Here, W/F is defined as the catalyst weight divided by the gas flow rate. CO_2 was the only detectable C-containing product, which initially passed through the TDX-01 stainless steel packed column, and then converted to methane in a reformer furnace; no significant amount of any partial oxidation product was detected in the effluent. The reactant and product were analyzed with an on-line gas chromatograph equipped with two flame ionization detectors (FID) in series. The yield of CO_2 (Y_{CO2}) was calculated according to the following formula:

$$Y_{Co_2} = 100 \times Co_{2\,out}/8/o - xylene_{in}$$

2.3. Materials characterization

The materials were characterized by powder X-ray diffraction (XRD), N_2 sorptometry, thermogravimetric analysis (TGA), X-ray photoelectron spectrometry (XPS), scanning electron microscopy (SEM) and high resolution transmission electron microscopy (HRTEM). XRD measurements were carried out in a Bruker AXS-D8 -ADVANCE using Cu Kα radiation and operated at 40 kV and 40 mA. The nitrogen adsorption–desorption isotherm was obtained at −196 °C using a Quantachrome NOVA 4000e instrument. Brunauer–Emmett–Teller (BET) method was used to calculate the surface area. The pore diameter distributions were calculated from desorption branches using the Barrett–Joyner–Halenda (BJH) method. Thermal stability and phase transitions were analyzed by TGA using a STA449F3 thermogravimetric analyzer (25–820 °C) at a heating rate of 10 °C/min in air atmosphere. The oxidation state of Mn in the product was measured by XPS using a SHIMADZU ESCA-3400 spectrometer (Mg Kα_radiation). The C1 s (284.6 eV) binding energy (BE) was used as internal reference. The binding energy regions of Mn2p and O1s were 630–670 eV, 522–542 eV respectively. The morphology of the material was observed using SEM on Hitachi S-4800 microscope. The product was further examined with transmission electron microscopy (TEM; H-600) and high-resolution transmission electron microscopy (HRTEM; JEM-2100, JEOL, Japan) operated at 200 kV.

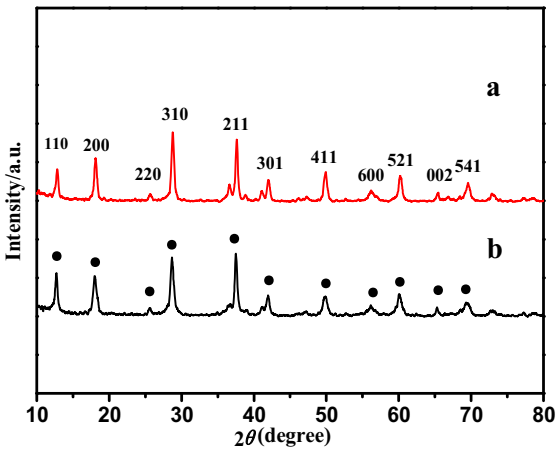

Fig. 1. XRD patterns of (a) B-OMS-2; (b) N-OMS-2.

2.4. H_2-TPR and O_2-TPO

H_2 temperature-programmed reduction (H_2-TPR) and O_2 temperature-programmed oxidation (O_2-TPO) were conducted on a PCA-1200 multifunctional adsorption apparatus equipped with a TCD detector. 0.04 g of the OMS-2 sample was loaded in a quartz reactor. A silica gel particle trap was placed in front of the detector to adsorb water. Before the TPR analysis, the OMS-2 samples were pretreated at 300 °C in Ar at a flow rate of 40 mL/min for 1 h. TPR was performed by heating the pretreated OMS-2 sample at a rate of 10 °C/min to 600 °C in 10 vol% H_2/Ar at a flow rate of 30 mL/min. After the TPR analysis, the OMS-2 sample was treated in Ar at 25 °C for 0.5 h. Then TPO analysis was performed by heating the OMS-2 sample at a rate of 10 °C/min to 300 °C (avoiding the decomposition of O_2 in the OMS-2) in a 5 vol% O_2/He at a flow rate of 30 mL/min.

3. Results and discussion

3.1. Structural and textural properties of B-OMS-2 and N-OMS-2

Powder XRD analysis (Fig. 1) shows that both B-OMS-2 and N-OMS-2 materials display typical manganese oxide octahedral molecular sieve (OMS-2) crystal phase (JCDPS 44-0141, tetragonal, I4/m, a = b = 0.978 nm, c = 0.286 nm). The pattern of the OMS-2 can be indexed to the planes of {110}, {200}, {220}, {310}, {211}, {411}, {600}, {521}, {002} and {541} at 2θ = 12.8°, 18.1°, 25.8°, 37.6°, 41.9°, 49.8°, 60.1°, 65.7° and 69.4° respectively [16]. The intensity of

Please cite this article in press as: Y. Wu, et al., Effect of reducing agent on the structure and activity of manganese oxide octahedral molecular sieve (OMS-2) in catalytic combustion of *o*-xylene, Catal. Today (2016), http://dx.doi.org/10.1016/j.cattod.2016.05.024

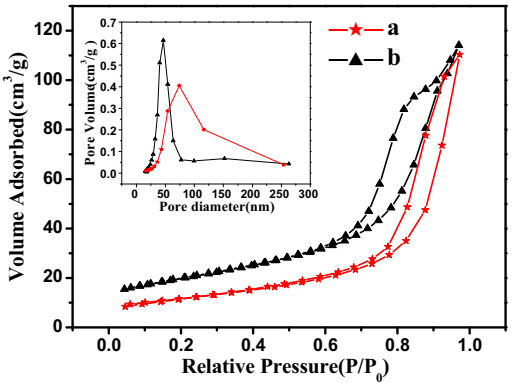

Fig. 2. N_2 adsorption–desorption isotherms and Barret–Joyner–Halenda (BJH) pore size distribution plots (inside) of (a) B-OMS-2; (b) N-OMS-2.

the {200} plane of B-OMS-2 was slightly higher than that of {110} plane, indicating more {200} plane exposure, which is consistent with the HRTEM result (see below in Fig. 4b).

The BET surface area and pore volume of B-OMS-2 are 40.65 $m^2 g^{-1}$ and 0.17 $cm^3 g^{-1}$, respectively, similar to those of N-OMS-2 (40.98 $m^2 g^{-1}$ and 0.17 $cm^3 g^{-1}$). However, the pore size of N-OMS-2 is only 46.52 nm, significantly smaller than that of B-OMS-2 (73.98 nm). These results indicated that different reducing agent led to a difference in pore size. Chen et al. found that the aggregation process plays an important role in tailoring the features of the porous structure in the product [21]. For B-OMS-2, the formation of MnOx nuclei is slow due to the hydrophobicity of benzyl alcohol, which gave a chance for benzyl alcohol molecules to adsorb on the MnOx. And the adsorbate hindered the aggregation of MnOx nuclei. When benzyl alcohol was removed in the calcination process, large pore was formed.

The nitrogen adsorption isotherms and the pore size distributions are shown in Fig. 2. It can be concluded that N-OMS-2 is typically type-IV with hysteresis loops, which means that the material presents a mesoporous structure, with a pore size distributions concentrated at (50.0 nm). Whereas, the B-OMS-2 exhibited large mesopores or macropores with a widepore size distributions concentrated at 50–100 nm.

Fig. 3 showed the SEM images of the N-OMS-2 and B-OMS-2. The texture and morphology of the two materials are significantly different. The N-OMS-2 consists of large and closely packed spherical particles with particle size of 200–500 nm (Fig. 3b left). The B-OMS-2 presents a loose structure, which is composed of a series of unequal-sized nanocubes. (Fig. 3a left). EDX spectra (Fig. 3a,b right) reveal that the two materials are composed of Mn, O, as well as K. B-OMS-2 has higher K contents than N-OMS-2.

TEM (Fig. 4) further confirmed the packed nanoparticles morphology of N-OMS-2 and loose nanocubes morphology of the B-OMS-2. The HRTEM images showed that the N-OMS-2 nanoparticles maintained two kinds of interlayer distance of 0.49 nm and 0.69 nm, respectively. These lattice distances agree well with the lattice spacing of the {200} and {110} crystal planes. While, B-OMS-2 nanocubes showed only {200} crystal plane.

Chemical species located in the region near the catalysts surface is characterized by XPS. The deconvolution of Mn $2p_{3/2}$ and Mn $2p_{1/2}$ signal is known to be useful to distinguish the oxidation states of $Mn^{\delta+}$ and the results are shown in Fig. 5. The binding energies

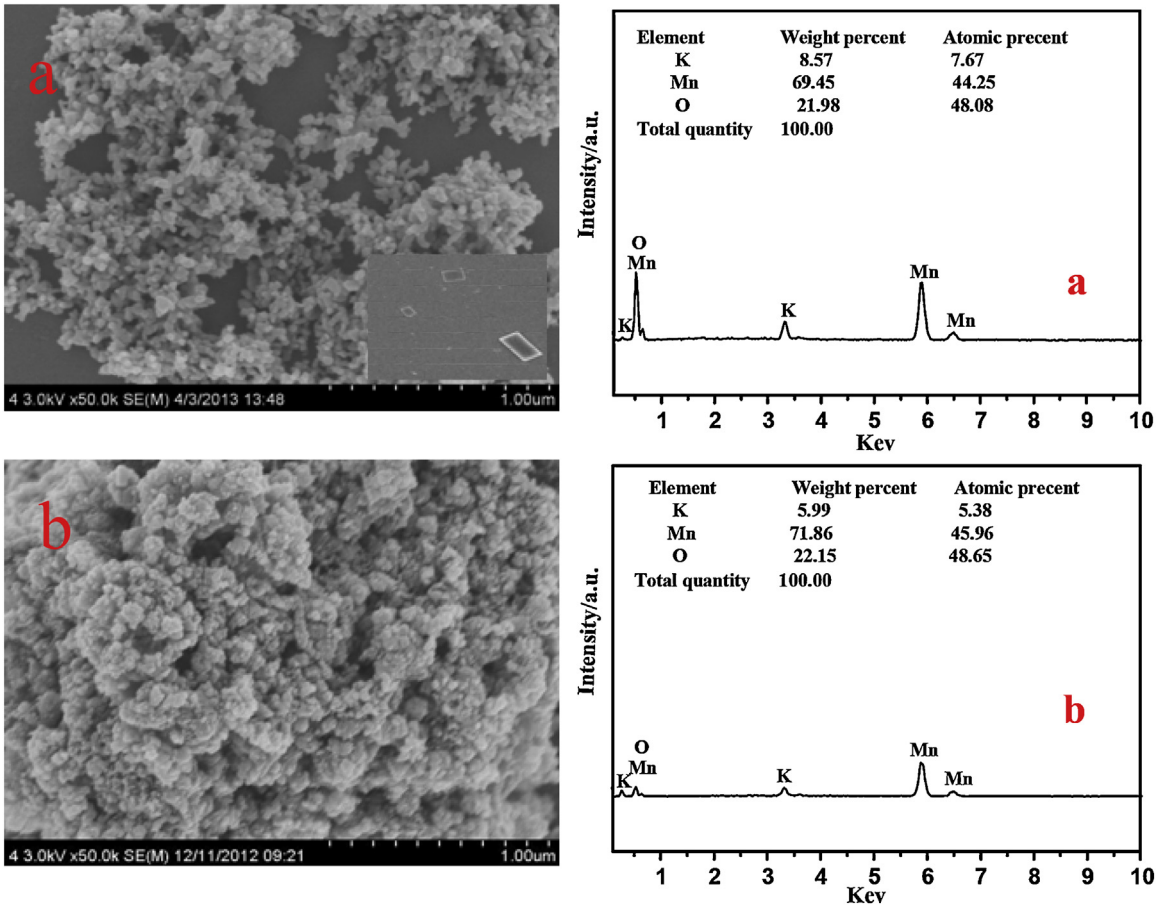

Fig. 3. SEM images and EDX patterns of (a) B-OMS-2; (b) N-OMS-2.

Please cite this article in press as: Y. Wu, et al., Effect of reducing agent on the structure and activity of manganese oxide octahedral molecular sieve (OMS-2) in catalytic combustion of *o*-xylene, Catal. Today (2016), http://dx.doi.org/10.1016/j.cattod.2016.05.024

Table 1
XPS and AOS results of B-OMS-2 and N-OMS-2 samples.

Samples	BE(eV)		$Mn^{4+}/(Mn^{3+}+Mn^{4+})$(%)	BE(eV)			$O\alpha/(O\alpha+O\beta+O_\gamma)$	AOS[a]
	Mn^{3+}	Mn^{4+}		Oα	Oβ	O_γ		
B-OMS-2	0	642.42	100	529.70	531.45	–	78.96	3.96
N-OMS-2	641.73	642.23	61.84	529.35	531.83	533.40	32.28	3.55

[a] The AOS is obtained by the results of chemical titration.

of Mn 2p3/2 at 639.9–640.3 eV, 640.5–641.9 eV and 642.0–642.5 eV can be ascribed to Mn^{2+}, $Mn^{3+}$and Mn^{4+} ions, respectively [7,10]. Table 1 summarized the percentage of different Mn oxidation states, and different oxygen types. It can be seen that the two materials have significantly different $Mn^{4+}/Mn^{3+}$and O_{latt}/O_{surf} ratios, which was caused by the different reducing agent used, For B-OMS-2, only Mn^{4+} can be detected on its surface. Although the shape of Mn2p 3/2 signal for both samples is very similar, the signal intensity of N-OMS-2 is weaker than that of B-OMS-2. Moreover, for N-OMS-2, there is an obvious shift of the $Mn2p_{3/2}$ peak towards lower binding energy (from 642.0 eV to 641.6 eV), which indicates that Mn^{4+} and Mn^{3+} species are coexisted in the sample. The $Mn^{4+}/Mn^{4+}+Mn^{3+}$ ratio is shown in Table 1. From chemical titration, the average oxidation state (AOS) of B-OMS-2 and N-OMS-2 were calculated to be 3.55 and 3.96, respectively. Based on the principle of electroneutrality, it can be deduced that there is some surface oxygen vacancy on the N-OMS-2 surface. According to the previous report [22], this kind of oxygen vacancy was defined as Mn^{3+}-oxygen vacancy associates. The result is agreement with the following O1 s analysis.

The chemical environment of oxygen in metal oxide catalysts played an important role in their catalytic properties. Fig. 5(B) shows the XPS spectra of O1 s in B-OMS-2 and N-OMS-2. For N-OMS-2, three peaks were observed, attributing to three types of oxygen species: the peak at BE of 529–530 eV was ascribed to the lattice oxygen in Mn-O-Mn (denoted as Oα), the peak at BE of 531–532 eV was ascribed to surface adsorbed oxygen, surface oxygen ions with low coordination Mn-O-H and oxygen vacancies (denoted as Oβ), and the peak at a higher BE (above 533 eV) corresponded to adsorbed molecular water (denoted as O_γ) [23]. The relative amount of Oα, Oβ and O_γ in N-OMS-2 were about 1/3 for each respectively. As for B-OMS-2, it possesses almost 100% Mn^{4+}. However, the peak deconvolution of O1 s indicate that both Oα and Oβ species exist in it. The relative amount of Oα in B-OMS-2 is 78.96% (see Table 1). 100% Mn^{4+} content generally corresponds to the absence of Oβ. The reason may be that the bond of Mn-O is weak due to the existence of bulk oxygen vacancy. It might lead to the formation of more labile oxygen species in the sample. Therefore, the BE of some lattice oxygen might be close to surface adsorbed oxygen. In addition, it is found that the binding energy of Mn $2p_{3/2}$ and the lattice oxygen shift to higher level compared to those of N-OMS-2. Qu et al. investigated the effects of Ag on Mn/SBA-15 catalysts, and found that Ag enters into MnO_2 phase and caused the presence of a defect in manganese, leading to an increase in the binding energy of O1s [7]. Therefore, it can be deduced that there are some structural defects in B-OMS-2.

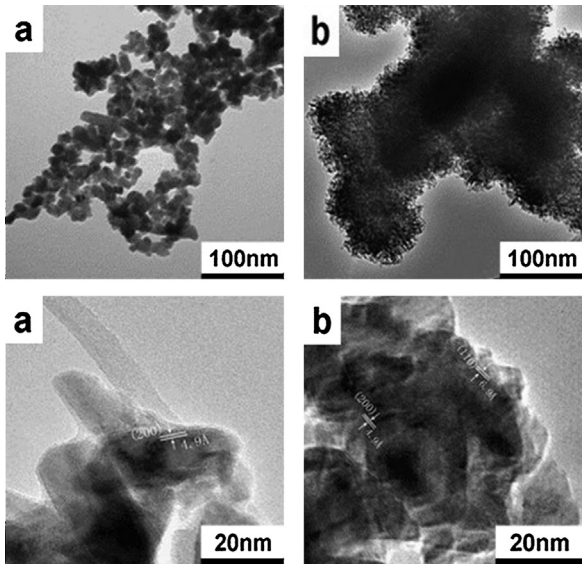

Fig. 4. TEM and HRTEM images of (a) B-OMS-2; (b) N-OMS-2.

3.2. Thermal stability of B-OMS-2 and N-OMS-2

The TGA profiles of N-OMS-2 and B-OMS-2 in the temperature range of 25 and 800 °C in air are presented in Fig. 6. Usually, thermal

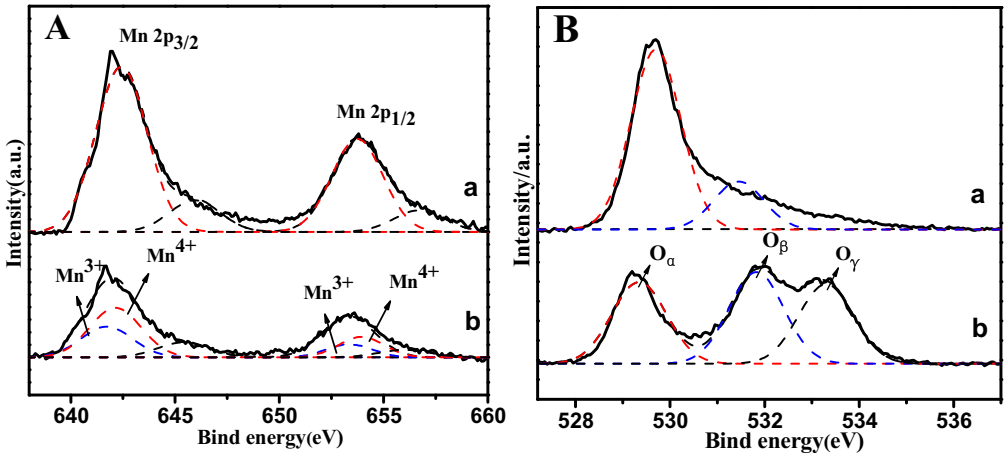

Fig. 5. Mn 2p XPS spectra (A) and O 1s XPS spectra (B) of B-OMS-2 (a) and N-OMS-2 (b).

Please cite this article in press as: Y. Wu, et al., Effect of reducing agent on the structure and activity of manganese oxide octahedral molecular sieve (OMS-2) in catalytic combustion of *o*-xylene, Catal. Today (2016), http://dx.doi.org/10.1016/j.cattod.2016.05.024

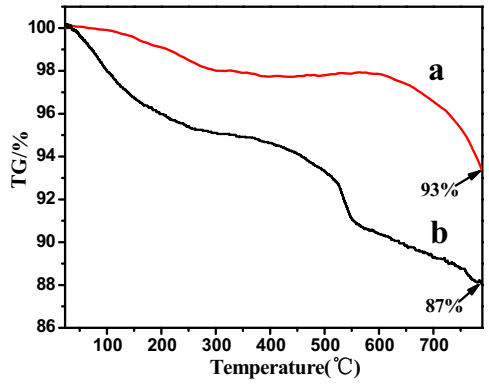

Fig. 6. TGA curves of OMS-2 treatment under air: (a) B-OMS-2; (b) N-OMS-2.

analysis of manganese oxides (MnO_2)in air presents three thermal features: (a) loss of physically adsorbed molecular water in the temperature range 100–200 °C; (b) loss of chemically bound water and a change of crystalline phase between 200 and 400 °C; and (c) the transformation of MnO_2 to Mn_2O_3 around 550 °C. The weight loss above 800 °C is attributed to the phase transformation of MnO_2 to Mn_3O_4 [24,25]. The total (physically and chemically bound) water losses for B-OMS-2 and N-OMS-2 were 2.0% and 5.0%, respectively. The water losses of N-OMS-2 were much larger than that of B-OMS-2, in accordance with the XPS results that show abundant water molecules exist in N-OMS-2. Moreover, in the temperature range of 400–800 °C, N-OMS-2 exhibited a more obvious crystalline phase change from MnO_2 to Mn_2O_3 and then to Mn_3O_4 than that of B-OMS-2.

Theoretically, the weight loss for the phase transformation of MnO_2 to Mn_3O_4 is 13%. This is what was observed for N-OMS-2. However, only 7% weight loss was observed for B-OMS-2, 1/2 of the theoretic value. The lower weight loss suggested that there are lower valence state Mn ions and/or oxygen vacancies in B-OMS-2. In order to prove this hypothesis, B-OMS-2 was calcined at temperatures of 500, 600, and 650 °C for 4 h to investigate their phase transformation. XRD results confirmed that B-OMS-2 is stable even above 650 °C. The results of XPS and chemical titration also showed that only Mn^{4+} exist sin B-OMS-2. These results indicated there may be some bulk oxygen vacancies in the B-OMS-2 lattice. Luo et al. also reported that, for OMS-2, the evolution of oxygen could lead to the formation of framework oxygen vacancies without destroying its structure [8]. Based on XPS and TGA results, we suggested that some oxygen vacancies exist in B-OMS-2.We denoted this kind of oxygen defects as bulk oxygen vacancy in order to distinguish it from the Mn^{3+}-oxygen vacancy associates in N-OMS-2.

It is worth noting that a weight increase occurred after 450 °C for B-OMS-2. Fig. 6 shows that B-OMS-2 achieved its maximum weight increase (0.2%) at 690 °C due to an oxygen gain, and a quick weight loss due to oxygen evolution subsequently occurred at 710 °C. N-OMS-2 did not exhibit any weight increase during the whole TGA profile; only weight losses of water and oxygen were observed. The results indicated that B-OMS-2 might have high oxygen exchange ability in air due to the existence of bulk oxygen vacancies, which is also supported by the subsequent O_2-TPO measurement result (see Fig. 7B below). This is in agreement with Zhang and Suib's results [26].

3.3. H_2-TPR and O_2-TPO of B-OMS-2 and N-OMS-2

H_2 temperature-programmed reduction (H_2-TPR) has been used extensively in the literature to characterize the surface and bulk oxygen reducibility of oxide materials.

According to the Mars-van Krevelen mechanism, the redox property of MnO_2 is also related to its re-oxidation ability. In this work, we interrupted the H_2-TPR at 600 °C, the samples were re-oxidized with 5% O_2/He at 25 °C, and then O_2-TPO analysis was performed.

Fig. 7A showed the H_2-TPR profiles of B-OMS-2 and N-OMS-2. The reduction curve of N-OMS-2 is the typical feature of two step reduction of MnO_2. The low-temperature reduction peak centered at *ca.* 273 °C represented the reduction of MnO_2 to Mn_2O_3 and the high-temperature reduction peak at 343 °C referred to the further reduction of Mn_2O_3 to MnO [14]. However, for B-OMS-2, only one main reduction band centered at 315 °C along with a wide shoulder peak ranging from 230 °C to 270 °C was observed. The shoulder peak reveals the presence of the labile oxygen species with weak Mn–O bond strength. This may support the XPS result, which indicates the existence of some surface oxygen species. The main reduction curve indicates the direct reduction of MnO_2 to MnO [14]. TPR results show that N-OMS-2 has a relatively high reducibility in the low temperature, which may be due to its large amount of surface oxygen. Whereas, the reduction rate of B-OMS-2 is faster than that of N-OMS-2. TPR analysis shows that the redox behavior of the manganese oxide in B-OMS-2 was potent, indicating a high reducibility or lattice oxygen mobility.

It is known that the catalytic activity is also closely related to the oxygen adsorption capacity and refreshment of lattice oxygen of the catalyst. To reveal the re-oxidation capability, a series of O_2-TPO tests were carried out. Fig. 7B showed the TPO profiles of B-OMS-2 and N-OMS-2 after H_2-TPR reduction. For B-OMS-2, there are one strong O_2 consumption peak and two small peaks at 170, 215 °C and 253 °C, respectively. According to the H_2-TPR analysis, the peaks at 170, 215 °C may be assigned to two-step reoxidation for B-OMS-2 pre-reduced by H_2: Mn_3O_4 to MnO_2 and MnO to Mn_3O_4,

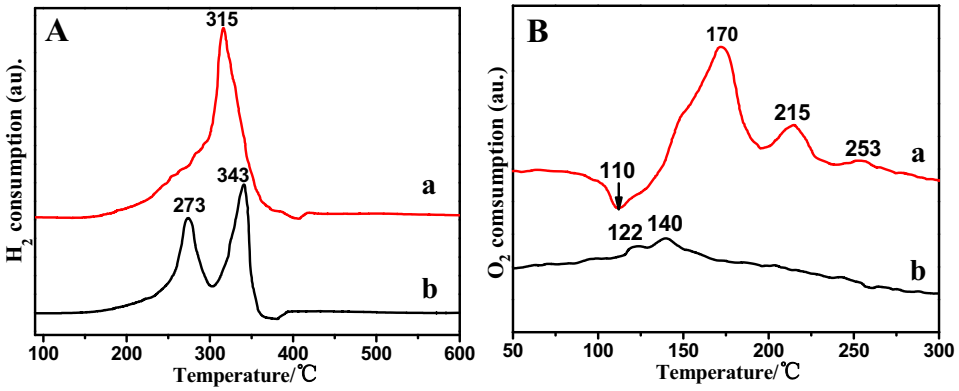

Fig. 7. H_2-TPR (A) and O_2-TPO(B) profiles of (a) B-OMS-2 and (b) N-OMS-2. The signal intensities of O_2-TPO are enlarged 10 times.

Please cite this article in press as: Y. Wu, et al., Effect of reducing agent on the structure and activity of manganese oxide octahedral molecular sieve (OMS-2) in catalytic combustion of *o*-xylene, Catal. Today (2016), http://dx.doi.org/10.1016/j.cattod.2016.05.024

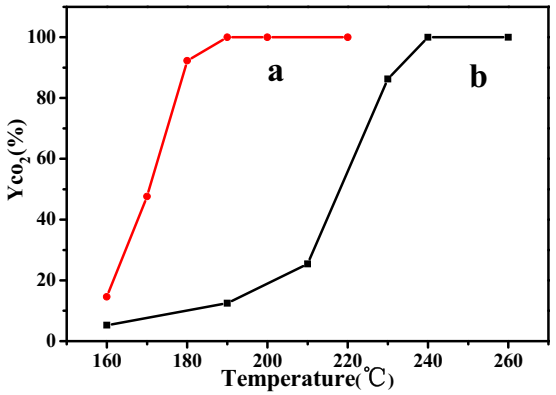

Fig. 8. CO_2 yield over B-OMS-2 (a) and N-OMS-2 (b). Reaction conditions: *o*-xylene 500 ppm, 20% O_2/N_2 balance, total flow rate 50 mL/min, W/F = 0.60 g s mL^{-1}.

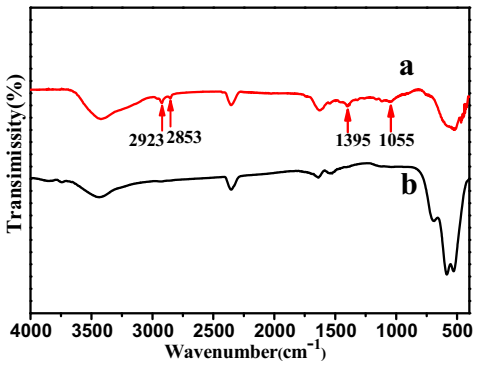

Fig. 9. FT-IR spectra of B-OMS-2: (a) dried at 110 °C, (b) calcined at 400 °C.

respectively [5]. The weak peak at 253 °C indicates that there are gas phase oxygen adsorption/exchange sites in B-OMS-2. There is also a small surface O_2 spillover peak appeared at 110 °C, indicating surface oxygen release without reaction in H_2-TPR.

For N-OMS-2, it starts to be re-oxided at ~122 °C and 142 °C. The reoxidation temperature is much lower than that of B-OMS-2, and the O_2 consumption peak area was smaller. These phenomena demonstrate that the O_2 adsorption properties and the oxygen exchange ability of B-OMS-2 and N-OMS-2 are different at temperatures less than 300 °C. The larger O_2 consumption on B-OMS-2 means that the interaction between B-OMS-2 and the gas phase oxygen is stronger than that of N-OMS-2. That is to say, B-OMS-2 exhibits stronger adsorption properties and higher exchange ability with gas phase oxygen than N-OMS-2 does.

3.4. o-*Xylene catalytic oxidation over B-OMS-2 and N-OMS-2*

The catalytic performance of B-OMS-2 and N-OMS-2 are evaluated in the *o*-xylene catalytic oxidation and the results are presented in Fig. 8. It is clearly seen that B-OMS-2 performed much better than the N-OMS-2 catalyst, indicating that the microstruture significantly influences the catalytic activity of OMS-2 for *o*-xylene oxidation. 100% CO_2 yield was observed at 190 °C for B-OMS-2, while for N-OMS-2, 100% CO_2 yield was observed at 240 °C, 50 °C higher than B-OMS-2. The performance of B-OMS-2 is comparable to some precious metals [3]. To examine the catalytic stability of B-OMS-2 sample, we carried out the on-stream reaction experiment at 190 °C (the result is not shown here). No significant decrease in catalytic activity was observed within 60 h of on-stream reaction. Hence, we believe that B-OMS-2 was catalytically durable.

In the past years, a number of materials have been used as catalysts for the oxidative removal of *o*-xylene. It was reported that for the combustion of *o*-xylene, the $T_{90\%}$ value was 249 °C over the Pd/Co_3O_4 catalyst at WHSV = 60 000 mL/(g h) [3], 240 °C over the Mn-Ce oxides catalyst at GHSV = 8000 h^{-1} [27], 220 °C over α-MnO_2 catalyst at GHSV = 8000 h^{-1} [28]. Apparently, the B-OMS-2 ($T_{90\%}$ value was 180 °C) catalyst outperformed the above-mentioned catalysts for the combustion of *o*-xylene.

It is well-known that the catalytic activity of manganese oxide is associated with several factors, such as surface area, Mn^{4+}/Mn^{3+} molar ratio, oxygen vacancy, and reducibility. For the combustion of organic compounds, the catalyst with a higher surface area would show a better catalytic activity. The surface area of B-OMS-2 is similar to that of N-OMS-2. However, B-OMS-2 significantly outperformed N-OMS-2, indicating that surface area was a minor factor influencing the catalytic performance.

In our previous studies, we have found that the surface concentration of Mn^{4+} ion plays an important role for its high catalytic activity for the catalytic combustion of *o*-xylene [28]. Because the relative amounts of Mn^{4+} ion can influence the surface properties and composition of MnO_2, such as the surface acid-base property, the contents of lattice oxides and surface hydroxy group. In order to exclude the effect of relative amounts of Mn^{4+} ion on the B-OMS-2 and N-OMS-2, we compared the catalytic performance of B-OMS-2 and RP-MnO_2 (our previous product, which possessed almost 100% Mn^{4+} ion on their surfaces [28]). The results showed that the catalyst (RP-MnOx (8-400)) showed 100% *o*-xylene conversion to CO_2 at 210 °C, 20 °C higher than that of B-OMS-2. In view of the difference of the surface area of B-OMS-2 and RP-MnO_2, the areal rates of the two samples were calculated. The data were 2.90×10^{-8} and 1.27×10^{-9} mol m^{-2} min^{-1} for B-OMS-2 and RP-MnO_2 at 170 °C. The results indicate that Mn^{4+} ion species was also not the main factor for its catalytic activity. There may be other factors determining the B-OMS-2 activity.

Tang et al. found that the insertion of vanadium in the framework of OMS-2 may create surface defect sites in the manganese oxide structure, which enhances the activity of OMS-2 for HCHO catalytic oxidation [29]. Qu et al. also reported that doping Ag in manganese oxides resulted in the presence of some defects in manganese, and these defective sites can be the active centers in the catalytic reaction since the oxygen species of the defective oxides tends to be easily released and transferred, enhancing the reactivity of catalysts in oxidation of VOCs [7]. This result indicates that any processing condition that favors the formation of more desirable oxygen vacancies/defects will result in enhanced redox ability of manganese oxide.

According to our XPS and TGA results, there are some bulk oxygen vacancies in B-OMS-2. The H_2-TPR and O_2-TPO analyses revealed that B-OMS-2 possesses higher lattice oxygen mobility and stronger re-oxidation ability than N-OMS-2. The results are in good agreement with the sequence of the catalytic performance of the two OMS-2 samples. The more surface oxygen content generally corresponds to higher activity in VOCs oxidation reaction. However, it is known that the catalytic activity is also closely related to the oxygen adsorption capacity and refreshment of lattice oxygen of the catalyst. In spite of B-OMS-2 having lower surface oxygen content, it showed high activity because it possesses more bulk oxygen vacancy. The presence of bulk oxygen vacancy enhances the reactivity of OMS by modifying the rate of vacancy exchange between the bulk and oxide surface. H_2-TPR and O_2-TPO results suggest that the bulk oxygen vacancy engenders higher lattice oxygen mobility and faster adsorption, diffusion and dissociation of gaseous oxygen at B-OMS-2 surface sites, which are able to explain its high *o*-xylene conversion activity. Therefore, we speculate that bulk oxygen vacancies in B-OMS-2 may be an important factor for its high catalytic activity. In addition, the loose structure and high K ion content may also play some roles.

Please cite this article in press as: Y. Wu, et al., Effect of reducing agent on the structure and activity of manganese oxide octahedral molecular sieve (OMS-2) in catalytic combustion of o-xylene, Catal. Today (2016), http://dx.doi.org/10.1016/j.cattod.2016.05.024

3.5. The possible formation mechanism of bulk oxygen vacancy in B-OMS-2

The formation of bulk oxygen vacancy is related to the microstructure of OMS-2. Usually, the growth of primary structures is modulated by preferential adsorption of anions, solvent molecules, and different reaction conditions. Although the exact growth mechanism of the B-OMS-2 is not completely understood, we suggest that benzyl alcohol, the organic oxygen-containing functional group may act as anchoring sites or nucleation sites controlling the growth of B-OMS-2 nuclei. The formation mechanism of bulk oxygen vacancy may be as follows: (1) a water and oil two-phase system is formed when benzyl alcohol is dropwise added to $KMnO_4$ solution. (2) MnOx nuclei are formed slowly as the reaction going on. At the same time, benzyl alcohol might adsorb on the MnOx nuclei, and the adsorbate may function as a structure directing agent that is capable of retarding the aggregation of the building blocks. (3) A rapid and uniform evolution of oxygen-containing functional groups may occur as the sample is calcined at 400 °C, which lead to the formation of bulk oxygen vacancy. Suib and co-workers also found that some of the oxygen in the OMS-2 framework can easily dislodge from the framework and evolve into air without destroying the skeleton of the parent cryptomelane structure when the sample is heated in air at as high as 650 °C. The evolution of oxygen results in the formation of framework oxygen vacancies, which are catalytically active sites for the oxidation reactions. Our results may agree with the literatures [8,26].

Fig. 9 showed the FT-IR spectra of the product of $KMnO_4$/benzyl alcohol dried at 110 °C and calcined at 400 °C respectively. The product dried at 110 °C showed a clear C-H stretching and bend vibration bands at 2923, 2853, and 1395 cm^{-1}. Moreover, there is also a C-O stretching vibration band appear at 1055 cm^{-1}. The broadband at *ca.* 3400 cm^{-1} and 1638 cm^{-1} correspond to the stretching and bending vibrations of OH-groups, respectively. The IR result indicates the existence of aliphatic alcohol. The result supports the hypothesis that there are some organic compounds absorbed on the surface of MnO_2 nuclei in advance, which decompose to form small aliphatic alcohol in the subsequent heating process. When the product was calcined at 400 °C, the absorbed aliphatic alcohol disappeared. B-OMS-2 presents a clear signature at 527, 578 and 705 cm^{-1}, which are ascribed to the vibrations of the MnO_6 octahedral framework of OMS-2 as previously reported [19].

4. Conclusion

B-OMS-2 and N-OMS-2 samples were prepared via $KMnO_4$ as oxidizing agent and benzyl alcohol and $Mn(NO_3)_2$ as reducing agent respectively. The OMS-2 samples were used as catalysts for *o*-xylene removal. XRD, BET, FT-IR, SEM, TEM, HRTEM, XPS and TGA techniques revealed that there was a direct relationship between the reduced agent, the microstructure of the OMS-2 materials and their reactivity toward *o*-xylene removal. B-OMS-2 presented a loose structure and contained almost 100% Mn^{4+}. XPS and TGA results showed that there was some bulk oxygen vacancy in B-OMS-2. FT-IR verified that the adsorption and desorption of benzyl alcohol on the MnO_2 nuclei may result in the formation of the bulk oxygen vacancy. Whereas, N-OMS-2 presented a mixture of Mn^{4+} and Mn^{3+}, indicating there exist small Mn^{3+}-oxygen vacancy associates. H_2-TPR and O_2-TPO results showed that B-OMS-2 exhibited high reducibility and oxygen exchange ability with gas phase oxygen. The activity test results showed that B-OMS-2 could convert 100% *o*-xylene into CO_2 at 190 °C at a space velocity of 8000 h^{-1}, 50 °C lower than N-OMS-2. It is concluded that the bulk oxygen vacancy, high reducibility and re-oxidation ability may be responsible for B-OMS-2's excellent catalytic performance.

Acknowledgements

This work was financially supported by the National Natural Science Foundation of China (No. 21147004, No. 21201054), the Natural Science Foundation of Hebei Province (No. B2013205100, No. 2013205136), and the Natural Science Foundation of Hebei Education Department (No. ZD2015114).

References

[1] W.X. Tang, X.F. Wu, S.D. Li, X. Shan, G. Liu, Y.F. Chen, Appl. Catal. B 162 (2015) 110–121.
[2] S.J. Jiang, E.S. Handberg, F. Liu, Y.T. Liao, H.Y. Wang, Z. Li, S.Q. Song, Appl. Catal. B 160–161 (2014) 716–721.
[3] Y.F. Wang, C.B. Zhang, Y.B. Yu, R.L. Yue, H. He, Catal. Today 242 (2015) 294–299.
[4] J. Spivey, Ind. Eng. Chem. Res. 26 (1987) 2165–2175.
[5] J.T. Hou, L.L. Liu, Y.Z. Li, M.Y. Mao, H.Q. Lv, X.J. Zhao, Environ. Sci. Technol. 47 (2013) 13730–13736.
[6] H. Sun, S. Chen, P. Wang, X. Quan, Chem. Eng. J. 178 (2011) 191–196.
[7] Z.P. Qu, Y.B. Bu, Y. Qin, Y. Wang, Q. Fu, Appl. Catal. B 132–133 (2013) 353–362.
[8] J. Luo, Q.H. Zhang, A. Huang, S.L. Suib, Microporous Mesopor. Mater. 35–36 (2000) 209–217.
[9] W.N. Li, J.K. Yuan, S. Gomez-Mower, S. Sithambaram, S.L. Suib, J. Phys. Chem. B 110 (2006) 3066–3070.
[10] F. Wang, H.X. Dai, J.G. Deng, G.M. Bai, K.M. Ji, Y.X. Liu, Environ. Sci. Technol. 46 (2012) 4034–4041.
[11] S. Dharmarathna, C.K. Kingondu, W. Pedrick, L. Pahalagedara, S.L. Suib, Chem. Mater. 24 (2012) 705–712.
[12] C.K. Kingondu, N. Opembe, C.H. Chen, K. Ngala, H. Huang, A. Iyer, H.F. Garces, S.L. Suib, Adv. Funct. Mater. 21 (2011) 312–323.
[13] J.T. Hou, Y.Z. Li, L.L. Liu, L. Ren, X.J. Zhao, J. Mater. Chem. A 1 (2013) 6736–6741.
[14] H.C. Genuino, S. Dharmarathna, E.C. Njagi, M.C. Mei, S.L. Suib, J. Phys. Chem. C 116 (2012) 12066–12078.
[15] S.K. Meher, G.R. Rao, J. Phys. Chem. C 117 (2013) 4888–4900.
[16] C.K. King'ondu, N. Opembe, C.H. Chen, K. Ngala, H. Huang, A. Iyer, H.F. Garcés, S.L. Suib, Adv. Funct. Mater. 21 (2011) 312–323.
[17] B.X. Hu, C.H. Chen, S.J. Frueh, L. Jin, R. Joesten, S.L. Suib, J. Phys. Chem. C 114 (2010) 9835–9844.
[18] J.H. Li, R.H. Wang, J.M. Hao, J. Phys. Chem. C 114 (2010) 10544–10550.
[19] H. Tian, J.H. He, X.D. Zhang, L. Zhou, D.H. Wang, Microporous Mesopor. Mater. 138 (2011) 118–122.
[20] Y.T. Wang, A.H. Lu, H.L. Zhang, W.C. Li, J. Phys. Chem. C 115 (2011) 5413–5421.
[21] W. Xiao, D. Hu, C. Peng, G.Z. Chen, Appl. Mater. Interfaces 3 (2011) 3120–3129.
[22] X.W. Liu, K.B. Zhou, L. Wang, B.Y. Wang, Y.D. Li, J. Am. Chem. Soc. 131 (2009) 3140–3141.
[23] V.P. Santos, M.F.R. Pereira, J.J.M. Órfão, J.L. Figueiredo, Appl. Catal. B 99 (2010) 353–363.
[24] L. Lamaita, M.A. Peluso, J.E. Sambeth, H.J. Thomas, Appl. Catal. B 61 (2005) 114–119.
[25] H. Sun, S. Chen, P. Wang, X. Quan, Chem. Eng. J. 178 (2011) 191–196.
[26] Q.H. Zhang, S.L. Suib, Chem. Mater. 11 (1999) 1306–1311.
[27] Y.S. Wu, Y.X. Zhang, M. Liu, Z.C. Ma, Catal. Today 153 (2010) 170–175.
[28] Y.S. Wu, Y. Lu, C.J. Song, Z.C. Ma, S.T. Xing, Y.Z. Gao, Catal. Today 201 (2013) 32–39.
[29] X.F. Tang, J.H. Li, J.M. Hao, Catal. Commun. 11 (2010) 871–875.

Please cite this article in press as: Y. Wu, et al., Effect of reducing agent on the structure and activity of manganese oxide octahedral molecular sieve (OMS-2) in catalytic combustion of *o*-xylene, Catal. Today (2016), http://dx.doi.org/10.1016/j.cattod.2016.05.024